Inorganic Chemistry

ARTICLE

pubs.acs.org/IC

Contrasting Reactivity and Cancer Cell Cytotoxicity of Isoelectronic Organometallic Iridium(III) Complexes

Zhe Liu, Luca Salassa, Abraha Habtemariam, Ana M. Pizarro, Guy J. Clarkson, and Peter J. Sadler*

Department of Chemistry, University of Warwick, Gibbet Hill Road, Coventry CV4 7AL, U.K.

Supporting Information

ABSTRACT: Replacing the N,N-chelating ligand 2,2′-bipyridine (bpy) in the Ir^{III} pentamethylcyclopentadienyl (Cp*) complex $[(\eta^5\text{-}C_5Me_5)Ir(bpy)Cl]^+$ (**1**) with the C,N-chelating ligand 2-phenylpyridine (phpy) to give $[(\eta^5\text{-}C_5Me_5)Ir(phpy)Cl]$ (**2**) switches on cytotoxicity toward A2780 human ovarian cancer cells (IC_{50} values of >100 μM for **1** and 10.8 μM for **2**). Ir−Cl hydrolysis is rapid for both complexes (hydrolysis equilibrium reached in <5 min at 278 K). Complex **2** forms adducts with both 9-ethylguanine (9-EtG) and 9-methyladenine (9-MeA), but preferentially with 9-EtG when in competition (ca. 85% of total Ir after 24 h). The X-ray crystal structure of $[(\eta^5\text{-}C_5Me_5)Ir(phpy)(9\text{-EtG-}N7)]NO_3\cdot 1.5CH_2Cl_2$ confirms N7 binding to guanine. Two-dimensional NMR spectra show that complex **2** binds to adenine mainly through N1, consistent with density functional theory (DFT) calculations. DFT calculations indicate an interaction between the nitrogen of the NH_2 group (9-MeA) and carbons from phpy in the adenine adduct of complex **2**. Calculations show that the most stable geometry of the adduct $[(\eta^5\text{-}C_5Me_5)Ir(phpy)(9\text{-EtG-}N7)]^+$ (**3b**) has the C6O of 9-EtG orientated toward the pyridine ring of phpy, and for $[(\eta^5\text{-}C_5Me_5)Ir(phpy)(9\text{-MeA-}N1)]^+$ (**4(N1)a**), the NH_2 group of 9-EtA is adjacent to the phenyl ring side of phpy. Complex **2** is more hydrophobic than complex **1**, with log *P* values of 1.57 and −0.95, respectively. The strong nucleobase binding and high hydrophobicity of complex **2** probably contribute to its promising anticancer activity.

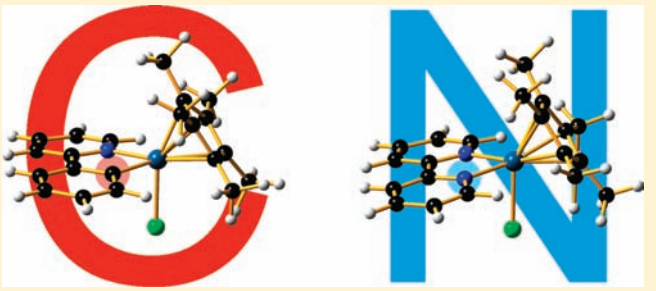

INTRODUCTION

Organometallic complexes offer rich versatility for the design of anticancer agents.[1] Iridium complexes are best known for their inertness,[2] and indeed inert organometallic Ir^{III} scaffolds are finding use as potent enzyme inhibitors.[3] The half-sandwich fragment $\{Cp^*Ir^{III}\}$ (Cp* = pentamethylcyclopentadienyl) has been used as a stabilizing entity in many organometallic iridium complexes.[4] By suitable choice of the other ligands, relatively reactive Cp* Ir^{III} complexes can be designed.[5] Here we focus attention on the role of the XY chelating ligand in $[(\eta^5\text{-}C_5Me_5)Ir(XY)Cl]^{0/+}$ complexes. Chelating ligands are already known to have a major influence on the DNA base specificity and cytotoxicity of organometallic half-sandwich complexes of the type $[(\eta^6\text{-arene})Ru/Os(XY)Z]$.[6] In a recent study we have shown that Cp* Ir^{III} complexes with XY = N,N-bound ethylenediamine, 2,2′-bipyridine, and 1,10-phenanthroline, or N,O-bound picolinate, are all inactive and noncytotoxic toward A2780 human ovarian cancer cells, all with IC_{50} values (concentrations at which 50% of the cell growth is inhibited) of >100 μM.[5] Also Cp* PTA iridium(III) complexes (PTA = 1,3,5-triaza-7-phosphatricyclo-[3.3.1.1]decane)[7] and Cp* pyTz iridium(III) complexes (pyTz = 2-(pyridine-2-yl)thiazole)[8] are reported to be inactive against A2780 cells (IC_{50} values >300 μM). Sheldrick et al. have shown that activity can be switched on by incorporating a DNA intercalator (N,N-chelating polypyridyl ligand) into some Cp* Ir^{III} complexes.[9] Here we introduce a different switch involving a single atom change (C^- for N) in a chelating 2,2′-bipyridine ligand to afford a neutral complex.

Cyclometalated organometallic complexes incorporating C,N-chelating ligands have attracted much attention because of their wide applications in both catalysis and luminescence.[10] However, few such previous studies have involved their anticancer activity.[11] In the work reported here, we compare the structure, reactivity, and cancer cell cytotoxicity of Cp* Ir^{III} complexes containing a neutral N, N-bound 2,2′-bipyridine (bpy) chelating ligand and an anionic C,N-bound 2-phenylpyridine (phpy) ligand. We have studied the hydrolysis, nucleobase binding, and hydrophobicity (octanol/water partition), and attempted to relate these to their activity toward A2780 ovarian cancer cells. This appears to be the first report of an active Ir^{III} anticancer complex containing both Cp* and a C,N-chelating ligand. This class of iridium complexes is attractive for development as new anticancer agents.

EXPERIMENTAL SECTION

Materials. $IrCl_3\cdot nH_2O$, 9-ethylguanine (9-EtG), 9-methyladenine (9-MeA), 2,2′-bipyridine, 2-phenylpyridine, octan-1-ol (≥99%), and NaCl (>99.999%) were purchased from Sigma-Aldrich. Nitric acid (72%) from Sigma Aldrich was double distilled and diluted using double deionized water. Complexes $[(\eta^5\text{-}C_5Me_5)Ir(bpy)Cl]Cl$ (**1**)[4a] and

Received: March 24, 2011
Published: May 27, 2011

   dx.doi.org/10.1021/ic200607j | *Inorg. Chem.* 2011, 50, 5777–5783

$[(\eta^5\text{-}C_5Me_5)Ir(phpy)Cl]$ (**2**)[12] were prepared according to literature methods. Details of the synthesis and characterization of complex $[(\eta^5\text{-}C_5Me_5)Ir(phpy)(9\text{-EtG-}N7)]NO_3$ (**3**·NO_3) are in the Supporting Information.

X-ray Crystallography. Diffraction data for **3**·NO_3·$1.5CH_2Cl_2$ were obtained on an Oxford Diffraction Gemini four-circle system with a Ruby CCD area detector using Mo Kα radiation. Absorption corrections were applied using ABSPACK.[13] The crystals were mounted in oil and held at 100(2) K with the Oxford Cryosystem Cobra. The structures were solved by direct methods using SHELXS (TREF)[14] with additional light atoms found by Fourier methods. Complexes were refined against F^2 using SHELXL,[15] and hydrogen atoms were added at calculated positions and refined riding on their parent atoms.

Crystallographic data are shown in Table S1 in the Supporting Information, and selected bond lengths and angles are listed in Table S2 in the Supporting Information. There is one CH_2Cl_2 molecule in a general position in the cell and one CH_2Cl_2 molecule that straddles a cell face. X-ray crystallographic data for **3**·NO_3·$1.5CH_2Cl_2$ are available as Supporting Information and have been deposited in the Cambridge Crystallographic Data Centre under the accession number CCDC 816981.

NMR Spectroscopy. ^{1}H NMR spectra were acquired in 5 mm NMR tubes at 310 K (unless stated otherwise) on either Bruker DPX 400 (^{1}H = 400.03 MHz) or AVA 600 (^{1}H = 600.13 MHz) spectrometers. ^{1}H NMR chemical shifts were internally referenced to CHD_2-OD (3.33 ppm) for methanol-d_4 or to 1,4-dioxane (3.75 ppm) for aqueous solutions. All data processing was carried out using XWIN-NMR version 3.6 (Bruker U.K. Ltd.).

Mass Spectrometry. Electrospray ionization mass spectra (ESI-MS) were obtained by infusing the samples into a Bruker Esquire 2000 mass spectrometer. The mass spectra were recorded with a scan range of m/z 50−1000 for positive ions.

Elemental Analysis. CHN elemental analyses were carried out on a CE-440 elemental analyzer by Exeter Analytical (U.K.) Ltd.

Computational Details. The Gaussian 03 package[16] was employed for all calculations. Geometry optimization calculations for complexes **1** and **2**, their aqua derivatives, and their 9-ethylguanine (9-EtG) and 9-ethyladenine (9-EtA) adducts were performed in the gas phase with the hybrid functional PBE1PBE.[17] 9-EtA was chosen instead of 9-MeA (used in experimental work) for the sake of comparison in the density functional theoretical (DFT) work. The LanL2DZ basis set and effective core potential[18] were used for the Ir atom, and the 6-31G** basis set was used for all other atoms.[19] The nature of all stationary points was confirmed by performing a normal-mode analysis. Electrostatic potential surfaces (EPSs) for complexes **1** and **2**, their aqua derivatives, and their 9-EtG and 9-EtA adducts were calculated and mapped on electron density (isovalue 0.04) of the molecules. The electrostatic potential is represented with a color scale ranging from red (−0.500 au) to blue (0.500 au). DFT results are summarized in the Supporting Information.

Interactions with Nucleobases. The reaction of complexes **1** and **2** (ca. 1 mM) with nucleobases typically involved addition of a solution containing 1 mol equiv of nucleobase in D_2O to an equilibrium solution of complexes **1** and **2** in 10% MeOD-d_4/90% D_2O (v/v). The pH* value (pH meter reading without correction for effects of deuterium on the glass electrode) of the sample was adjusted if necessary to remain close to 7.4 (physiological pH). The reaction of equimolar amounts of complex **1** with 9-MeA was carried out in MeOD-d_4 (ca. 7 mM) to provide concentrations high enough for the two-dimensional (2D) NMR work. ^{1}H NMR spectra, 2D ^{1}H−^{1}H TOCSY, and NOESY of these solutions were recorded at 310 K after various time intervals.

Formation constants for nucleobase complexes, K = [bound 9-EtG or 9-MeA][free Cl^-]/[free 9-EtG or 9-MeA][free iridium complex], are based on NMR peak integrals.

Chart 1. Iridium(III) Pentamethylcyclopentadienyl Complexes Studied in This Work[a]

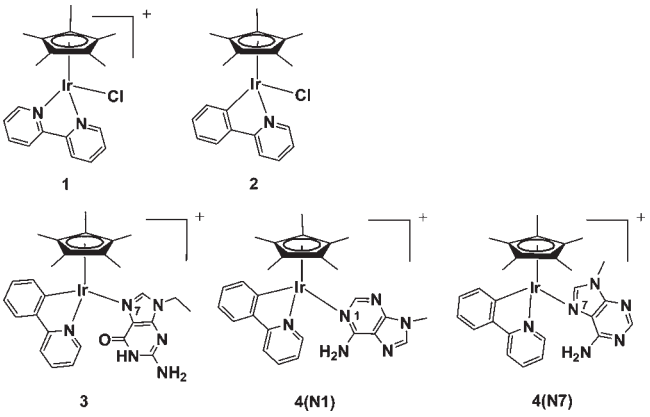

[a]Complex **1** was isolated as a Cl^- salt; complexes **3**, **4(N1)** and **4(N7)** were isolated as NO_3^- salts.

Inductively Coupled Plasma Mass Spectrometric (ICP-MS) Instrumentation and Calibration. All ICP-MS analyses were carried out on an Agilent Technologies 7500 series ICP-MS instrument. The water used for ICP-MS analysis was doubly deionized (DDW) using a Millipore Milli-Q water purification system and a USF Elga UHQ water deionizer. The iridium Specpure plasma standard (Alfa Aesar, 1000 ppm in 10% HCl) was diluted with 3% HNO_3 DDW to freshly prepare calibrants at concentrations of 1000, 800, 400, 200, 100, 50, 10, 1, and 0.1 ppb. The ICP-MS instrument was set to detect ^{193}Ir with a typical detection limit of ca. 2 ppt using no-gas mode.

log *P* Determination. Octanol-saturated water (OSW) and water-saturated octanol (WSO) were prepared using analytical grade octanol and 0.2 M NaCl aqueous solution (to suppress hydrolysis of the chlorido complexes). Aliquots of stock solutions of iridium complexes in OSW were added to equal volumes of WSO and shaken in an IKA Vibrax VXC basic shaker for 4 h at 500 g/min, ∼298 K, to allow partition at ambient temperature (shake-flask method). The aqueous layer was carefully separated from the octanol layer for iridium analysis. ^{193}Ir was quantified from aliquots taken from the octanol-saturated aqueous samples before and after partition. Partition coefficients of Ir^{III} complexes were calculated using the equation log P = log $([Ir]_{WSO}/[Ir]_{OSW})$, where $[Ir]_{WSO}$ was obtained by subtraction of the Ir content of the aqueous layer after partition from the Ir content of the aqueous layer before partition.

Cytotoxicity. The A2780 human ovarian cancer cell line was obtained from the ECACC (European Collection of Animal Cell Cultures, Salisbury, U.K.). The cells were maintained in RPMI 1640 media (supplemented with 10% fetal calf serum, 1% L-glutamine, and 1% penicillin/streptomycin). All cells were grown at 310 K in a humidified atmosphere containing 5% CO_2. Stock solutions of the Ir^{III} complexes were first prepared in DMSO to assist dissolution (maximum final DMSO concentration 1.25% v/v), and then diluted into 0.9% saline and medium (1:1). After plating 5000 A2780 cells per well on day 1, Ir^{III} complexes were added to the cancer cells on day 3 at concentrations ranging from 0.5 to 100 μM. Cells were exposed to the complexes for 24 h, washed with PBS, supplied with fresh medium, and allowed to grow for three doubling times (72 h). Protein content (proportional to cell survival) was then determined using the sulforhodamine B (SRB) assay.[20] The standard errors are based on two independent experiments carried out in triplicate.

RESULTS AND DISCUSSION

We have investigated the chemical reactivity and cancer cell cytotoxicity of the isoelectronic complexes $[(\eta^5\text{-}C_5Me_5)Ir(bpy)Cl]^+$ (**1**) and $[(\eta^5\text{-}C_5Me_5)Ir(phpy)Cl]$ (**2**), which contain 2,2′-bipyridine

dx.doi.org/10.1021/ic200607j |*Inorg. Chem.* 2011, 50, 5777–5783

Table 1. Selected Bond Distances (Å) for $[(\eta^5\text{-}C_5Me_5)Ir(bpy)Cl]^+$ (1) and $[(\eta^5\text{-}C_5Me_5)Ir(phpy)Cl]$ (2) Calculated at the PBE1PBE/LANLD2Z/6-31G Level**

complex	Ir−Cl	Ir−N1/C1	Ir−N2	Ir−Centroid
1	2.398	2.083	2.083	1.816
2	2.411	2.009	2.077	1.863
1 (X-ray)[4a]	2.404(2)	2.076(8)	2.090(9)	1.786
2 (X-ray)[12]	2.3968(7)	2.046(2)	2.080(2)	1.820

and 2-phenylpyridine as N,N- and C,N-chelating ligands, respectively (Chart 1), including hydrolysis, nucleobase binding, and DFT calculations. The syntheses and X-ray structures of both complexes have been reported previously.[4a,12]

Structural and Electronic Differences between Complexes 1 and 2. There is a change in the overall charge on the complex from positive for complex **1**, where the chelating ligand is N,N-bound 2,2′-bipyridine, to neutral for complex **2**, which contains C,N-bound 2-phenylpyridine. Geometry optimization calculations for complexes **1** and **2** were performed using the PBE1PBE functional. Selected bond distances for $[(\eta^5\text{-}C_5Me_5)Ir(bpy)Cl]^+$ (**1**) and $[(\eta^5\text{-}C_5Me_5)Ir(phpy)Cl]$ (**2**) are listed in Table 1 and are in good agreement with the reported X-ray crystal structures.[4a,12] In complex **2**, the chelating ligand is closer to the Ir^{III} center than in complex **1**; a short Ir−C(phenyl) distance causes elongation of the Ir−Cl bond as well as the Ir−Cp*(centroid) distance (Table 1). The same features are observed for the aqua adducts of complexes **1** and **2** (Table S3 in the Supporting Information) and their 9-EtG and 9-EtA adducts (Tables S4 and S5 in the Supporting Information, respectively).

Details of the frontier orbitals and electrostatic potential surfaces (EPSs) of complexes **1** and **2**, their aqua adducts, and their 9-EtG and 9-EtA adducts are in the Supporting Information (Tables S6−S8 and Figure S1). No significant differences or unexpected features are observed for the frontier orbitals of these derivatives or for their EPSs.

Hydrolysis. Hydrolysis of M−Cl bonds is often an activation step for transition metal anticancer complexes.[21] We have previously reported that complex **1** undergoes rapid hydrolysis.[5] The hydrolysis of complex **2** (1 mM) in 10% MeOD-d_4/90% D_2O (v/v) was studied by ^{1}H NMR spectroscopy. The presence of methanol ensured sufficient solubility of the complex. Complex **2** underwent fast hydrolysis even at 278 K. Any difference in the hydrolysis rates of complexes **1** and **2** could not be determined since the hydrolysis equilibria were reached by the time the first ^{1}H NMR spectrum was acquired (~5 min). At equilibrium ca. 32% of complex **2** was in the hydrolyzed form. To confirm the hydrolysis of **2**, NaCl was added to an equilibrium solution containing the chlorido complex **2** and its aqua adduct **2_D$_2$O** (Figure 1A) to give concentrations of 4, 23, and 104 mM NaCl, mimicking the chloride concentrations in the cell nucleus, cell cytoplasm, and blood plasma, respectively.[22] ^{1}H NMR spectra were then recorded within 10 min of the additions at 298 K. With addition of NaCl, ^{1}H NMR peaks corresponding to the chlorido complex **2** increased in intensity while peaks for the aqua adduct **2_D$_2$O** decreased in intensity; see Figure 1B. These data confirm the formation of the aqua adduct and the reversibility of the process. On the basis of ^{1}H NMR peak integrals, almost no hydrolyzed complex **2** was found to be present in 104 mM $[Cl^-]$ or in 23 mM $[Cl^-]$, and <5% of aqua complex **2_D$_2$O** was observed at 4 mM $[Cl^-]$ after 10 min with no further change after

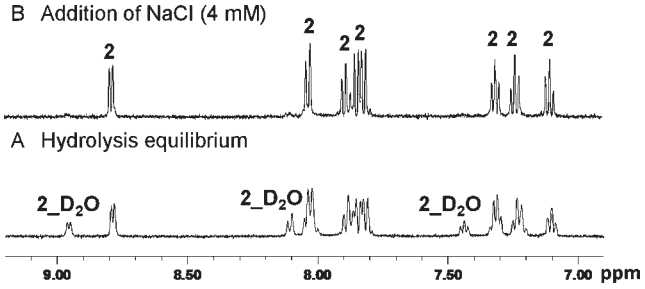

Figure 1. Hydrolysis of $[(\eta^5\text{-}C_5Me_5)Ir(phpy)Cl]$ (**2**). Low-field region of the ^{1}H NMR spectrum of (A) an equilibrium solution of **2** (1 mM) in 10% MeOD-d_4/90% D_2O (v/v) at 298 K and (B) 10 min after addition of NaCl (4 mM). The peaks for the chlorido complex **2** increased in intensity, while peaks for the aqua complex $[(\eta^5\text{-}C_5Me_5)Ir(phpy)(D_2O)]^+$ (**2_D$_2$O**) decreased upon addition of NaCl.

24 h. Therefore hydrolysis is readily suppressed by NaCl, even at a chloride concentration close to that of the cell nucleus.

The fast hydrolysis can be related to the presence of the five methyl groups on the Cp ring as strong electron donors which increase the electron density on the Ir center and facilitate chloride loss. A similar hydrolysis behavior was observed for complex **1**[5] and for some hexamethylbenzene Ru^{II} complexes (compared to unsubstituted benzene complexes).[23]

Interactions with Nucleobases. Since binding to DNA is often associated with the cytotoxic activity of metal anticancer drugs,[24] reactions of complex **2** (1 mM) in 10% MeOD-d_4/90% D_2O (pH* 7.4) at 310 K with 1 mol equiv of the nucleobases 9-ethylguanine (9-EtG) and 9-methyladenine (9-MeA) were investigated. The extent of nucleobase adduct formation and relative formation constant for complexes **1** and **2** based on ^{1}H NMR peak integrals are shown in Table 2.

Addition of 1 mol equiv of 9-EtG to an equilibrium solution of complex **2** resulted in 96% formation of the G adduct, $[(\eta^5\text{-}C_5Me_5)Ir(phpy)(9\text{-EtG})]^+$ (**3**). The ^{1}H NMR spectrum of the reaction mixture in 10% MeOD-d_4/90% D_2O at 310 K showed a new 9-EtG H8 peak at 7.46 ppm, shifted by 0.37 ppm to high field relative to that of free 9-EtG. ESI-MS studies on the diluted sample (0.2 mM) gave a major peak at m/z 661.2 (Figure S2 in the Supporting Information), consistent with the presence of $[(\eta^5\text{-}C_5Me_5)Ir(phpy)(9\text{-EtG})]^+$ (calculated m/z 661.1). The formation constant K for the 9-EtG adduct of complex **2** is ca. 144 times that of complex **1**.

The 9-EtG adduct of complex **2**, $[(\eta^5\text{-}C_5Me_5)Ir(phpy)(9\text{-EtG})]NO_3$, **3·NO$_3$**, was isolated, and the X-ray crystal structure confirmed that 9-EtG is bound through N7 (Figure 2A). The nitrate counterion shows H-bonding to a 9-EtG ligand, with distances of 1.987(19) Å (O12···H26) and 1.975(19) Å (O10···H27A) (Figure 2B and Table S9 in the Supporting Information). The H-bonded chains are linked by two hydrogen bonds N27−H27B···N28 (2.105(19) Å) between two symmetrical guanines. From a search of the Cambridge Crystallographic Data Centre database, this appears to be the first example of an X-ray structure of a guanine adduct containing a chiral iridium center.

Addition of 1 mol equiv of 9-MeA to an equilibrium solution of complex **2** in 10% MeOD-d_4/90% D_2O at 310 K resulted in ca. 86% of **2** reacting with 9-MeA after 24 h. Two adenine nucleobase adducts are formed in a 4.5:1 ratio as indicated by ^{1}H NMR, and correspond to iridium binding to N1 and N7 of adenine, **4(N1)** and **4(N7)** (Chart 1). ESI-MS studies on the diluted sample (0.2 mM)

dx.doi.org/10.1021/ic200607j |Inorg. Chem. 2011, 50, 5777–5783

Table 2. Formation Constants for 9-EtG and 9-MeA Adducts of Complexes 1 (1 mM) and 2 (1 mM) at 310 K after 24 h (in 10% MeOD-d_4/90% D_2O), log *P* Values, and IC_{50} Values for A2780 Human Ovarian Cancer Cell Line for Complexes 1 and 2

	9-EtG adduct		9-MeA adduct			A2780[a,b]
complex	%	*K*	%	*K*	log *P*	IC_{50} (μM)
1	61[c]	1.6	0[c]		-0.95 ± 0.06	>100[c]
2	96	230.4	86	6.1	1.57 ± 0.08	10.8 ± 1.7

[a] Cisplatin IC_{50} as control 1.2 ± 0.1 μM. [b] Drug-treatment period was 24 h. [c] Ref 5.

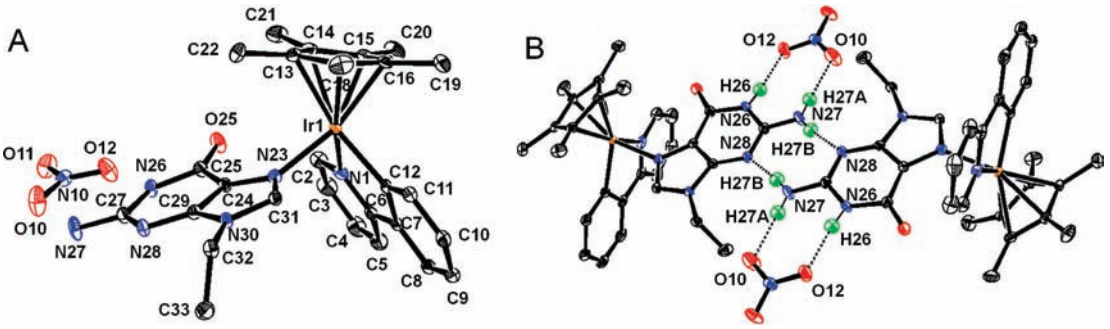

Figure 2. X-ray crystal structure of $[(\eta^5\text{-}C_5Me_5)Ir(phpy)(9\text{-EtG-}N7)]NO_3 \cdot 1.5CH_2Cl_2$ ($\mathbf{3 \cdot NO_3} \cdot 1.5CH_2Cl_2$). (A) Atom numbering scheme. Only the cation and anion are shown for clarity. (B) Formation of dimers linked by N27−H27B···N28 hydrogen bonds of 9-EtG (2.105(19) Å). The NO_3^- counteranions form H-bonds with N26H and N27H (O12···H26 1.987(19) Å and O10···H27A 1.975(19) Å).

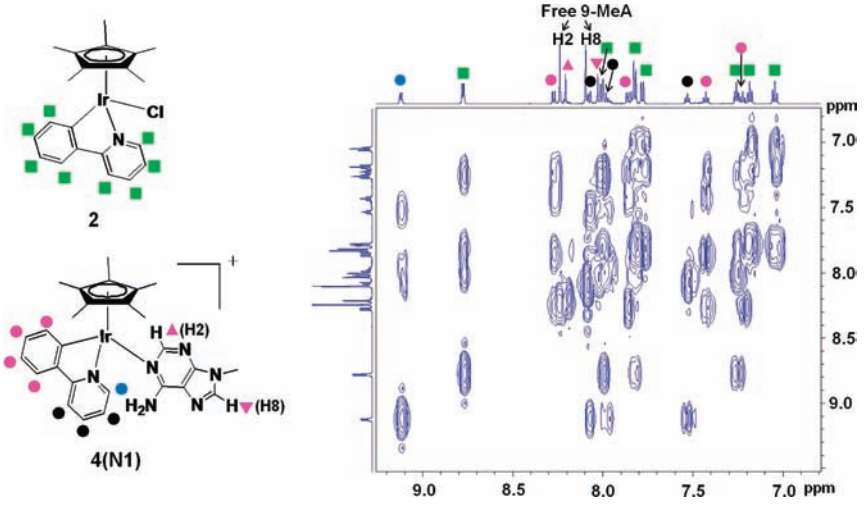

Figure 3. $^1H-^1H$ TOCSY 2D NMR spectrum of an equimolar equilibrium solution of 9-MeA and complex **1** (7 mM) in MeOD-d_4. Peak assignments are indicated on the structures.

gave a major peak at *m*/*z* 631.2 (Figure S3 in the Supporting Information), consistent with the formation of $[(\eta^5\text{-}C_5Me_5)Ir(phpy)(9\text{-MeA})]^+$ (calculated *m*/*z* 631.0).

To understand the mode of binding to adenine, 1:1 mol equiv of 9-MeA and complex **2** were dissolved in MeOD-d_4 (7 mM), and 2D $^1H-^1H$ TOCSY (Figure 3) and NOESY (Figure 4) spectra were recorded. Only 40% of complex **2** reacted with 9-MeA in MeOD-d_4 at 310 K after 24 h, which indicates that nucleobase binding in MeOD-d_4 was less favorable than in 10% MeOD-d_4/90% D_2O (86%, Table 2). This may be due to the poor solvation of the leaving chloride by MeOD-d_4 and lack of hydrolysis. Complex **2** also formed two 9-MeA adducts in a 6.6:1 ratio in MeOD-d_4 based on the integration of the Cp* ^1H NMR peaks. The ^1H NMR peaks of the minor adduct in the low-field region are weak and overlapped by the peaks of the major adduct (Figure 3). An NOE cross-peak between H2 of 9-MeA and the HC═N proton of phpy was observed (Figure 4), suggesting that coordination of 9-MeA through N1 is the major binding mode. This result is consistent with the DFT calculations which show that $[(\eta^5\text{-}C_5Me_5)Ir(phpy)(9\text{-EtA-}N1)]^+$ is more stable than $[(\eta^5\text{-}C_5Me_5)Ir(phpy)(9\text{-EtA-}N7)]^+$ by 18.36 kJ/mol (Table S5 in the Supporting Information).

The N7 atoms of G and A are accessible to metal ions, such as Pt in cisplatin,[25] for coordination in the major groove of DNA, whereas N1 of A is involved in Watson−Crick base pairing. Complex **2** reacted with guanine via N7 and formed adenine adducts via N1 and N7, with **4(N1)** being the major adenine adduct. In addition, complex **2** has a higher affinity for guanine

dx.doi.org/10.1021/ic200607j |*Inorg. Chem.* 2011, 50, 5777–5783

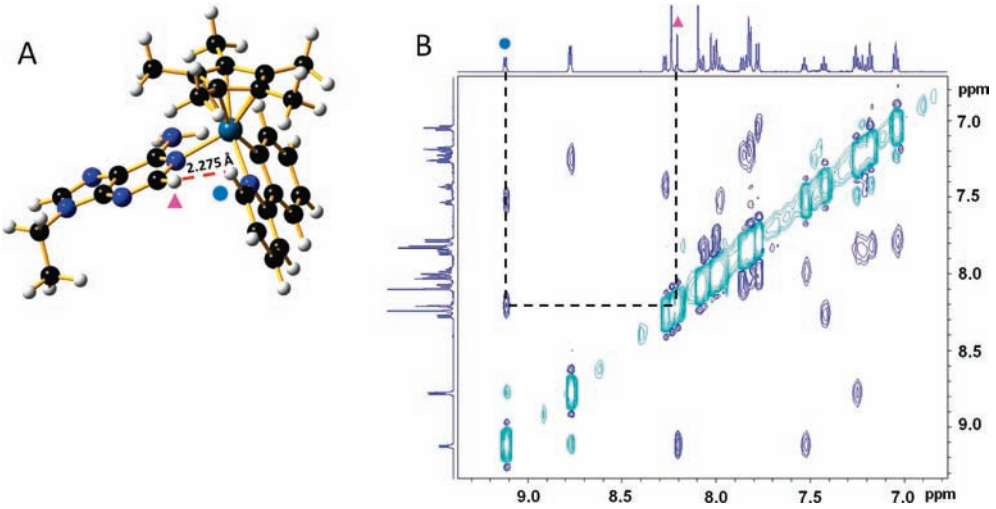

Figure 4. Model and 2D NOESY spectrum of $[(\eta^5\text{-}C_5Me_5)Ir(phpy)(9\text{-}EtA\text{-}N1)]^+$. (A) Optimized geometry showing a short distance of 2.275 Å between the HC═N proton of phpy (blue circle) and H2 of bound 9-MeA (pink triangle). (B) $^1H-^1H$ NOESY 2D NMR spectrum of adduct in the reaction mixture of complex **2** $[(\eta^5\text{-}C_5Me_5)Ir(phpy)Cl]$ with 1 mol equiv of 9-MeA (7 mM, MeOD-d_4), which confirms coordination of 9-MeA through N1 as the major binding mode.

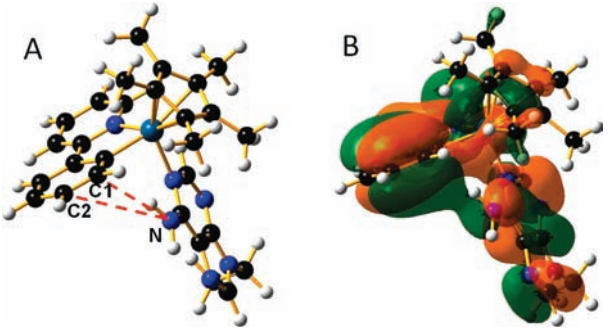

Figure 5. (A) DFT optimized structure of complex $[(\eta^5\text{-}C_5Me_5)Ir(phpy)(9\text{-}EtA\text{-}N1)]^+$. (B) HOMO − 2 orbital for the DFT-optimized complex $[(\eta^5\text{-}C_5Me_5)Ir(phpy)(9\text{-}EtA\text{-}N1)]^+$ showing the N(NH_2 of 9-EtA)···C1/C2(phpy) interactions.

compared to adenine. Binding to guanine may therefore play a more significant role in its cytotoxicity.

Compared with the C,N-chelated 2-phenylpyridine complex **2**, which binds significantly to both nucleobases, the N,N-chelated 2,2′-bipyridine complex **1** formed an adduct only with 9-EtG (61%), and not with 9-MeA after 24 h (Table 2), indicating weaker binding to both guanine and adenine bases.

The calculations suggest that there is a π orbital interaction between N (NH_2 of adenine) and C1 and C2 (phpy) for the DFT-optimized complex $[(\eta^5\text{-}C_5Me_5)Ir(phpy)(9\text{-}EtA\text{-}N1)]^+$ (Figure 5). This may explain the formation of adenine adducts $[(\eta^5\text{-}C_5Me_5)Ir(phpy)(9\text{-}MeA)]^+$ by complex **2**. These negatively charged carbons on the phenyl ring appear to be favored for such interactions compared with the analogous atoms in the pyridine ring where C1 is positively charged and C2 is slightly negative. Although complex **2** can form 9-MeA adducts in MeOD-d_4 and D_2O, which may be due to the influence of water on the stability of different tautomeric forms of DNA bases through hydrogen bonding interactions,[26] the adducts readily dissociate in $CDCl_3$, acetone-d_6, DMSO-d_6, and THF-d_8, indicating that they are relatively unstable in these solvents. The formation constant for the 9-MeA adduct ($K = 6.1$, in 10% MeOD-d_4/90% D_2O Table 2), is ca. 38 times smaller than that of the 9-EtG adduct. Competition between equal molar amounts of 9-EtG and 9-MeA for complex **2** (0.4 mM) in 10% MeOD-d_4/90% D_2O at 310 K (pH* 7.4) gave rise to the 9-EtG adduct as the major product (ca. 85%) after 24 h, confirming the higher affinity for the nucleobase guanine.

Some Ru^{II} and Ir^{III} complexes containing N,N-chelating ligands such as ethylenediamine and 1,10-phenanthroline have little affinity for adenine residues.[5,27] In contrast, organometallic complexes containing N,O-chelating ligands or O,O-chelating ligands such as picolinate and acetylacetonate bind to both guanine and adenine residues.[5,6c,28] However, some Os^{II} complexes containing picolinate derivatives show a strong preference for adenine.[29] The chelating ligands in these complexes appear to play an important role in the recognition of nucleobases, interacting especially with the C6O of guanine or the C6NH_2 of adenine, which can be rationalized in terms of H-bonding, nonbonding repulsive interactions between the chelating ligand and nucleobase substituents, and the electronic properties of the various nucleobase coordination sites.[30] The chelating ligands in the present work also have a significant effect on the selectivity of nucleobase binding. Complex **1** containing N,N-chelating 2,2′-bipyridine reacted only with 9-EtG, while complex **2** containing C,N-chelating 2-phenylpyridine formed both 9-EtG and 9-MeA adducts, preferentially binding to 9-EtG when in competition, which may result from the steric hindrance of the NH_2 group at the 6-position of the adenine ring. Some Pt^{II} antitumor complexes bearing C,N-chelating ligands also show strong binding to 9-EtG.[31]

Configurational Studies of G and A Adducts. We investigated the relative stabilities of isomers of the guanine and adenine adducts. For $[(\eta^5\text{-}C_5Me_5)Ir(phpy)(9\text{-}EtG\text{-}N7)]^+$ (**3**) two orientations of the carbonyl group with respect to the 2-phenylpyridine ring are possible. In **3a** the carbonyl group of 9-EtG is oriented toward the phenyl ring of the phpy ligand, and in **3b** the carbonyl group is on the pyridine side. In the crystal studied by X-ray diffraction, the complex adopts configuration **3b** (Figure 3A), with a NC−H···O6(EtG) distance of 2.265 Å. This result is consistent with the DFT calculations which show that **3b** is more stable than **3a** by 24.09 kJ/mol.

Similarly, the energies of configurations of $[(\eta^5\text{-}C_5Me_5)Ir(phpy)(9\text{-}MeA\text{-}N1)]^+$ with different orientations of the NH_2

dx.doi.org/10.1021/ic200607j |*Inorg. Chem.* 2011, 50, 5777–5783

group of 9-EtA in adducts of complexes **1** and **2** were optimized and compared (Table S5 in the Supporting Information). The DFT calculations show that, for $[(\eta^5\text{-}C_5Me_5)Ir(phpy)(9\text{-}MeA\text{-}N1)]^+$ (**4(N1)**), adduct **4(N1)a** (NH_2 group of 9-EtA on the phenyl ring side of the phpy ligand) is more stable than **4(N1)b** (NH_2 group on the pyridine ring side). This preference was confirmed in solution by the $^1H-^1H$ NOESY 2D NMR spectrum recorded in MeOD-d_4 (Figure 4). An NOE cross-peak was observed between the H2 of bound 9-MeA and the pyridine ring (mixing times 0.15−0.8 s). This configuration may be stabilized by the π orbital interaction between N (NH_2 of adenine)···C1/C2 (phpy) (Figure 5). The energies of these nucleobase adducts of complexes **1** and **2** are listed and compared in Table S5 in the Supporting Information.

Partition Coefficients (log *P*). Lipophilicity often correlates with cytotoxic potency and has therefore been used extensively in structure−activity correlations.[32] The octanol−water partition coefficients (log *P*) for complexes **1** and **2** were determined and are listed in Table 2. Instead of water alone, 0.2 M NaCl was used to suppress hydrolysis of the complexes. Complex **1** is positively charged and shows a negative log *P* value of −0.95 (partitions preferentially into water ca. 10-fold), while the neutral complex **2** is much more hydrophobic with a log *P* value of 1.57 (partitions preferentially into octanol ca. 30-fold) (Table 2). The difference in partition coefficients between complexes **1** and **2** is thus directly related to the difference in their charges.

The hydrophobicity and cancer cell activity correlate significantly in this study. Complex **1** $[(\eta^5\text{-}C_5Me_5)Ir(bpy)Cl]^+$ is less hydrophobic and inactive. Complex **2** $[(\eta^5\text{-}C_5Me_5)Ir(phpy)Cl]$ displays much higher hydrophobicity, and is cytotoxic. This hydrophobicity difference is likely to result in higher cancer cell uptake and contribute to the higher cytotoxicity of complex **2**.

For compounds in the Comprehensive Medicinal Chemistry (CMC) database, which is often used to validate new pharmacophores, log *P* values range between −0.4 and 5.6, with an average value of 2.52.[33] The log *P* value of 1.57 for complex **2** is within this range, while the log *P* of −0.95 for complex **1** is more negative; i.e., complex **1** may be too hydrophilic for optimum druglike properties.

Cytotoxicity. The cytotoxicity of complexes **1**[5] and **2** toward A2780 human ovarian cancer cells was investigated (Table 2). The IC_{50} value (concentration at which 50% of the cell growth is inhibited) for complex $[(\eta^5\text{-}C_5Me_5)Ir(bpy)Cl]^+$ (**1**) was >100 μM (and is thus deemed inactive). However, the 2-phenylpyridine complex **2** is relatively potent with an IC_{50} value of 10.8 μM (Table 2), comparable to that of carboplatin.[23] Complex $[(\eta^5\text{-}C_5Me_5)Ir(phpy)Cl]$ (**2**) appears to be the first reported active Ir^{III} anticancer complex with both Cp* and C,N-chelating ligand. The higher cancer cell cytotoxicity of complex **2** correlates with its higher hydrophobicity and stronger nucleobase binding compared to complex **1**.

Some square-planar Au^{III} complexes containing C,N-chelating phpy ligand have been reported to be more cytotoxic than cisplatin in vitro against MOLT-4 human leukemia and C2Cl2 mouse tumor cell lines,[11a,34] although the mechanisms of action of these complexes are unknown.

CONCLUSIONS

The goal of the present study was to design Cp* Ir^{III} complexes which are cytotoxic toward cancer cells. Here, we have shown for the first time that Cp* Ir^{III} complex **2** $[(\eta^5\text{-}C_5Me_5)Ir(phpy)Cl]$ containing C,N-bound 2-phenylpyridine as the chelating ligand can exhibit significant cytotoxic activity toward A2780 human ovarian cancer cells, in contrast to the inactive analogue complex **1** $[(\eta^5\text{-}C_5Me_5)Ir(bpy)Cl]^+$ containing N,N-bound 2,2′-bipyridine as chelating ligand. Both complexes hydrolyze rapidly in water (hydrolysis equilibrium reached within 5 min at 278 K), but aquation (substitution of Cl by H_2O) is suppressed totally in 104 and 23 mM saline. Complex **2** binds significantly both to 9-EtG and 9-MeA, with a preference for the former, whereas complex **1** binds only to 9-EtG and with moderate affinity. The X-ray structure $[(\eta^5\text{-}C_5Me_5)Ir(phpy)(9\text{-}EtG\text{-}N7)]NO_3\cdot 1.5CH_2Cl_2$ (**3**·NO_3·$1.5CH_2Cl_2$) is the first example of a guanine adduct with a chiral iridium center and confirms the binding of complex **2** to N7 of 9-EtG. No attempt was made to separate the enantiomers of **2** or its adducts in the present work. Two-dimensional TOCSY and NOESY NMR spectroscopies and DFT calculations confirm that complex **2** binds to 9-MeA mainly through N1 binding. DFT calculations showed that the NH_2 nitrogen of 9-MeA can form a π orbital interaction with carbons of the phpy ligand. X-ray crystallography and DFT calculations confirm that the adduct $[(\eta^5\text{-}C_5Me_5)Ir(phpy)(9\text{-}EtG\text{-}N7)]^+$ (**3b**, carbonyl group of bound 9-EtG on the pyridine side) and the adduct $[(\eta^5\text{-}C_5Me_5)Ir(phpy)(9\text{-}MeA\text{-}N1)]^+$ (**4(N1)a**, NH_2 group of bound 9-EtA on the phenyl ring side of phpy ligand) are the most stable 9-EtG and 9-MeA adducts of complex **2**. Complex **2** is more hydrophobic than complex **1**. The strong nucleobase binding ability and higher hydrophobicity of complex **2** may contribute to its lower IC_{50} value.

This work illustrates how the structure, chemical reactivity, and cancer cell cytotoxicity of the Cp* Ir^{III} complexes can be controlled by variation of the chelating ligands. The promising anticancer activity of the organometallic iridium(III) C,N-complex **2** provides a basis for further exploration of this new class of anticancer complexes.

ASSOCIATED CONTENT

Supporting Information. Details of X-ray crystallographic data, bond lengths, and angles (Table S1 and S2), calculated bond distances for all derivatives of complexes **1** and **2** (Tables S3−S5), electrostatic potential surfaces (EPSs) for complexes **1**, **2**, and all their derivatives (Table S6), frontier orbitals of complexes **1**, **2**, and all their derivatives (Table S7, S8, Figure S1), H-bonding of complex **3** (Table S9), ESI-MS studies of binding to nucleobases (Figures S2 and S3), complete ref 16, and X-ray crystallographic data in CIF format. This material is available free of charge via the Internet at http://pubs.acs.org.

AUTHOR INFORMATION

Corresponding Author

*E-mail: P.J.Sadler@warwick.ac.uk.

ACKNOWLEDGMENT

Z.L. was supported by a University of Warwick Research Scholarship, and L.S. was supported by ERC BIOINCMED and MC-IEF (220281 PHOTORUACD). We thank the ERC (Grant 247450 for P.J.S.), EPSRC, ORSAS, ERDF, and AWM for Science City funding, and members of EC COST D39 for stimulating discussions.

REFERENCES

(1) (a) *Medicinal Organometallic Chemistry*, 1st ed.; Topics in Organometallic Chemistry 32; Jaouen, G., Metzler-Nolte, N., Eds.;

Springer-Verlag: Heidelberg, Germany, 2010. (b) Fish, R. H. *Aust. J. Chem.* **2010**, *63*, 1505–1513. (c) Gasser, G.; Ott, I.; Metzler-Nolte, N. *J. Med. Chem.* **2010**, *54*, 3–25. (d) Suss-Fink, G. *Dalton Trans.* **2010**, *39*, 1673–1688. (e) Dyson, P. J.; Sava, G. *Dalton Trans.* **2006**, 1929–1933.(f) Bruijnincx, P. C. A.; Sadler, P. J. In *Advances in Inorganic Chemistry*; Rudi van, E., Hubbard, C. D., Eds.; Academic Press: 2009; Vol. 61, pp 1−62.

(2) (a) Marcon, G.; Casini, A.; Mura, P.; Messori, L.; Bergamo, A.; Orioli, P. *Metal-Based Drugs* **2000**, *7*, 195–200. (b) Messori, L.; Marcon, G.; Orioli, P.; Fontani, M.; Zanello, P.; Bergamo, A.; Sava, G.; Mura, P. *J. Inorg. Biochem.* **2003**, *95*, 37–46.

(3) Wilbuer, A.; Vlecken, D. H.; Schmitz, D. J.; Kräling, K.; Harms, K.; Bagowski, C. P.; Meggers, E. *Angew. Chem., Int. Ed.* **2010**, *49*, 3839–3842.

(4) (a) Youinou, M.-T.; Ziessel, R. *J. Organomet. Chem.* **1989**, *363*, 197–208. (b) Amouri, H.; Moussa, J.; Renfrew, A. K.; Dyson, P. J.; Rager, M. N.; Chamoreau, L.-M. *Angew. Chem., Int. Ed.* **2010**, *49*, 7530–7533.

(5) Liu, Z.; Habtemariam, A.; Pizarro, A. M.; Fletcher, S. A.; Kisova, A.; Vrana, O.; Salassa, L.; Bruijnincx, P. C. A.; Clarkson, G. J.; Brabec, V.; Sadler, P. J. *J. Med. Chem.* **2011**, *54*, 3011–3026.

(6) (a) van Rijt, S. H.; Sadler, P. J. *Drug Discovery Today* **2009**, *14*, 1089–1097. (b) Peacock, A. F. A.; Sadler, P. J. *Chem.—Asian J.* **2008**, *3*, 1890–1899. (c) Fernández, R.; Melchart, M.; Habtemariam, A.; Parsons, S.; Sadler, P. J. *Chem.—Eur. J.* **2004**, *10*, 5173–5179.

(7) Casini, A.; Edafe, F.; Erlandsson, M.; Gonsalvi, L.; Ciancetta, A.; Re, N.; Ienco, A.; Messori, L.; Peruzzini, M.; Dyson, P. J. *Dalton Trans.* **2010**, *39*, 5556–5563.

(8) Gras, M.; Therrien, B.; Süss-Fink, G.; Casini, A.; Edafe, F.; Dyson, P. J. *J. Organomet. Chem.* **2010**, *695*, 1119–1125.

(9) Schäfer, S.; Ott, I.; Gust, R.; Sheldrick, W. S. *Eur. J. Inorg. Chem.* **2007**, 3034–3046.

(10) (a) Hull, J. F.; Balcells, D.; Blakemore, J. D.; Incarvito, C. D.; Eisenstein, O.; Brudvig, G. W.; Crabtree, R. H. *J. Am. Chem. Soc.* **2009**, *131*, 8730–8731. (b) Lo, K. K.-W.; Louie, M.-W.; Zhang, K. Y. *Coord. Chem. Rev.* **2010**, *254*, 2603–2622.

(11) (a) Fan, D.; Yang, C.-T.; Ranford, J. D.; Vittal, J. J.; Foo Lee, P. *Dalton Trans.* **2003**, 3376–3381. (b) Ruiz, J.; Vicente, C.; de Haro, C.; Bautista, D. *Dalton Trans.* **2009**, 5071–5073. (c) Leung, S.-K.; Kwok, K. Y.; Zhang, K. Y.; Lo, K. K.-W. *Inorg. Chem.* **2010**, *49*, 4984–4995.

(12) Li, L.; Brennessel, W. W.; Jones, W. D. *J. Am. Chem. Soc.* **2008**, *130*, 12414–12419.

(13) *CrysAlis PRO*; Oxford Diffraction Ltd.: Abington, Oxfordshire, U. K., 2007.

(14) Sheldrick, G. M. *Acta Crystallogr.* **1990**, *A46*, 467–473.

(15) Sheldrick, G. M. *SHELXL-97*; University of Göttingen: Göttingen, Germany, 1997.

(16) Frisch, M. J.; et al. *Gaussian 03*, revision D.01; Gaussian Inc.: Wallingford, CT, USA, 2003.

(17) Adamo, C.; Barone, V. *J. Chem. Phys.* **1999**, *110*, 6158–6170.

(18) Hay, P. J.; Wadt, W. R. *J. Chem. Phys.* **1985**, *82*, 270–283.

(19) McLean, A. D.; Chandler, G. S. *J. Chem. Phys.* **1980**, *72*, 5639–5648.

(20) Skehan, P.; Storeng, R.; Scudiero, D.; Monks, A.; McMahon, J.; Vistica, D.; Warren, J. T.; Bokesch, H.; Kenney, S.; Boyd, M. R. *J. Natl. Cancer Inst.* **1990**, *82*, 1107–1112.

(21) Pizarro, A. M.; Habtemariam, A.; Sadler, P. J. In *Medicinal Organometallic Chemistry*, 1st ed.; Jaouen, G., Metzler-Nolte, N., Eds.; Topics in Organometallic Chemistry 32; Springer-Verlag: Heidelberg, Germany, 2010; pp 21−56.

(22) Martin, R. B. In *Cisplatin: Chemistry and Biochemistry of a Leading Anticancer Drug*; Lippert, B., Ed.; VHCA & Wiley-VCH: Zürich, Switzerland, 1999; pp 181−205.

(23) Wang, F.; Habtemariam, A.; van der Geer, E. P. L.; Fernández, R.; Melchart, M.; Deeth, R. J.; Aird, R.; Guichard, S.; Fabbiani, F. P. A.; Lozano-Casal, P.; Oswald, I. D. H.; Jodrell, D. I.; Parsons, S.; Sadler, P. J. *Proc. Natl. Acad. Sci. U.S.A.* **2005**, *102*, 18269–18274.

(24) (a) Zhang, C. X.; Lippard, S. J. *Curr. Opin. Chem. Biol.* **2003**, *7*, 481–489. (b) Deubel, D. V.; Lau, J. K.-C. *Chem. Commun.* **2006**, 2451–2453.

(25) Jung, Y.; Lippard, S. J. *Chem. Rev.* **2007**, *107*, 1387–1407.

(26) (a) Gu, J.; Leszczynski, J. *J. Phys. Chem. A* **1999**, *103*, 2744–2750. (b) Gorb, L.; Leszczynski, J. *J. Am. Chem. Soc.* **1998**, *120*, 5024–5032. (c) Gu, J.; Leszczynski, J. *J. Phys. Chem. A* **1999**, *103*, 577–584.

(27) Chen, H.; Parkinson, J. A.; Morris, R. E.; Sadler, P. J. *J. Am. Chem. Soc.* **2003**, *125*, 173–186.

(28) (a) Peacock, A. F. A.; Parsons, S.; Sadler, P. J. *J. Am. Chem. Soc.* **2007**, *129*, 3348–3357. (b) Melchart, M.; Habtemariam, A.; Parsons, S.; Sadler, P. *J. Inorg. Biochem.* **2007**, *101*, 1903–1912.

(29) van Rijt, S. H.; Peacock, A. F. A.; Johnstone, R. D. L.; Parsons, S.; Sadler, P. J. *Inorg. Chem.* **2009**, *48*, 1753–1762.

(30) Peacock, A. F. A.; Habtemariam, A.; Fernández, R.; Walland, V.; Fabbiani, F. P. A.; Parsons, S.; Aird, R. E.; Jodrell, D. I.; Sadler, P. J. *J. Am. Chem. Soc.* **2006**, *128*, 1739–1748.

(31) Ruiz, J.; Rodríguez, V.; Cutillas, N.; Espinosa, A.; Hannon, M. J. *J. Inorg. Biochem.* **2011**, *105*, 525–531.

(32) (a) Loh, S. Y.; Mistry, P.; Kelland, L. R.; Abel, G.; Harrap, K. R. *Br. J. Cancer* **1992**, *66*, 1109–1115. (b) Barbieri, R. *Inorg. Chim. Acta* **1992**, *191*, 253–259. (c) Mendoza-Ferri, M.-G.; Hartinger, C. G.; Eichinger, R. E.; Stolyarova, N.; Severin, K.; Jakupec, M. A.; Nazarov, A. A.; Keppler, B. K. *Organometallics* **2008**, *27*, 2405–2407. (d) Song, R.; Park, S. Y.; Kim, Y.-S.; Kim, Y.; Kim, S.-J.; Ahn, B. T.; Sohn, Y. S. *J. Inorg. Biochem.* **2003**, *96*, 339–345. (e) Gramatica, P.; Papa, E.; Luini, M.; Monti, E.; Gariboldi, M.; Ravera, M.; Gabano, E.; Gaviglio, L.; Osella, D. *J. Biol. Inorg. Chem.* **2010**, *15*, 1157–1169. (f) Leo, A. J. *Chem. Rev.* **1993**, *93*, 1281–1306. (g) Reithofer, M. R.; Bytzek, A. K.; Valiahdi, S. M.; Kowol, C. R.; Groessl, M.; Hartinger, C. G.; Jakupec, M. A.; Galanski, M.; Keppler, B. K. *J. Inorg. Biochem.* **2011**, *105*, 46–51.

(33) Ghose, A. K.; Viswanadhan, V. N.; Wendoloski, J. J. *J. Comb. Chem.* **1999**, *1*, 55–68.

(34) Fan, D.; Yang, C.-T.; Ranford, J. D.; Lee, P. F.; Vittal, J. J. *Dalton Trans.* **2003**, 2680–2685.